Journal for ImmunoTherapy of Cancer

Targeting immunosuppressive macrophages by CSRP2-regulated CCL28 signaling sensitizes hepatocellular carcinoma to lenvatinib

Changzhou Chen ,[1,2] Sheng Su,[1,2] Pengcheng Wang,[3] Xinming Ye,[1,2] Songyang Yu,[4] Yu Gong,[1,2] Zehuan Li,[1,2] Jia Li,[5] Zhiqiang Hu,[1,2] Xiaowu Huang[1,2,6]

To cite: Chen C, Su S, Wang P, *et al*. Targeting immunosuppressive macrophages by CSRP2-regulated CCL28 signaling sensitizes hepatocellular carcinoma to lenvatinib. *Journal for ImmunoTherapy of Cancer* 2025;**13**:e012201. doi:10.1136/jitc-2025-012201

► Additional supplemental material is published online only. To view, please visit the journal online (https://doi.org/10.1136/jitc-2025-012201).

Accepted 25 August 2025

For numbered affiliations see end of article.

Correspondence to
Dr Xiaowu Huang;
huang.xiaowu@zs-hospital.sh.cn

Dr Zhiqiang Hu;
huzhiqiang924@sina.com

ABSTRACT

Background Despite comparable survival benefit has been obtained, the drug resistance remarkably reduced lenvatinib clinical efficacy. Here, we aimed to identify the potential mechanism by which cysteine and glycine-rich protein 2 (CSRP2) regulates the development of hepatocellular carcinoma (HCC) and participates in the resistance to lenvatinib.

Methods We harnessed RNA sequencing, multiplex immunofluorescence staining, and hydrodynamic tail vein (HTV) injection HCC model to systematically explore the function of CSRP2 in HCC progression. To precisely delineate how immunosuppressive macrophages, influenced by CSRP2-regulated C-C motif chemokine ligand 28 (CCL28) signaling, respond to lenvatinib-induced cytotoxicity, we established an in vitro co-culture system and conducted functional cytotoxicity assays.

Results Using RNA sequencing, multiplex immunofluorescence staining and HTV injection HCC mouse model, we identified CSRP2 as one of the most significantly upregulated genes in HCC tissues. CSRP2 overexpression drives anti-lenvatinib resistance by inducing high levels of tumor-associated macrophages (TAMs) infiltration and reshaping an immunosuppressive microenvironment. Then flow cytometry, mass spectrometry and chromatin immunoprecipitation were conducted to clarify the underlying mechanism of CSRP2. We showed CSRP2 promotes phosphorylation of activating transcription factor 2 (ATF2) at Thr69/71, leading to the transcriptional activation of CCL28 expression. HCC-derived CCL28 recruits TAMs to drive immunosuppression and anti-lenvatinib tolerance. BI6901, a potent and selective CCR10 antagonist, blocked TAMs recruitment and enhanced T-cell activation. Combining CCR10 inhibition improved the therapeutic benefit of anti-lenvatinib in HCC.

Conclusions These results illustrate that CSRP2 regulates the tumor microenvironment to promote HCC growth and drive lenvatinib tolerance via the CSRP2/ATF2/CCL28 axis. Targeting this pathway could synergize with lenvatinib to treat HCC more effectively.

WHAT IS ALREADY KNOWN ON THIS TOPIC

⇒ Lenvatinib is a key treatment for advanced hepatocellular carcinoma (HCC), but resistance limits its effectiveness.
⇒ The molecular mechanisms of lenvatinib resistance in HCC are not fully understood.
⇒ While cysteine and glycine-rich protein 2 (CSRP2) has been implicated in various cancers, its role in liver cancer, particularly in relation to lenvatinib resistance, remains unclear.

WHAT THIS STUDY ADDS

⇒ This study identifies CSRP2 as a key driver of lenvatinib resistance in HCC.
⇒ CSRP2 activates the CSRP2/activating transcription factor 2/C-C motif chemokine ligand 28 axis, promoting tumor-associated macrophage (TAM) recruitment and M2 polarization, which exhibits an immunosuppressive TME that limits T-cell activation.
⇒ Our in vivo study shows that targeting this axis enhances lenvatinib efficacy, and CSRP2 expression can serve as a biomarker for predicting resistance.

HOW THIS STUDY MIGHT AFFECT RESEARCH, PRACTICE OR POLICY

⇒ This study suggests that CSRP2 could be developed as a biomarker to guide treatment decisions, with high CSRP2 expression indicating potential benefit from combination therapies targeting lenvatinib.
⇒ The CCR10 inhibitor BI6901, which blocks TAM recruitment, may be tested in clinical trials alongside lenvatinib for CSRP2-high patients.

INTRODUCTION

Primary liver cancer (PLC) ranks as the third leading cause of cancer-related deaths worldwide, with hepatocellular carcinoma (HCC) accounting for nearly 90% of cases.[1] Most patients with HCC present with advanced disease, necessitating systemic therapies.[2] Currently, first-line treatments include multikinase inhibitors such as sorafenib and lenvatinib, while regorafenib and cabozantinib are used in second-line settings. However, the limited understanding of the molecular landscape of HCC means that only a subset of patients benefits from these therapies.[3] Therefore, elucidating the molecular

pathways underlying drug resistance and identifying novel, effective biomarkers are critical for improving patient outcomes.

Cysteine and glycine-rich protein 2 (CSRP2), a member of the CSRP family, encodes a group of short LIM domain proteins (21 kDa) that play critical roles in cellular development and differentiation.[4] Aberrant expression of CSRP2 has been observed in various cancers, where it contributes to tumorigenesis.[5–8] Notably, elevated CSRP2 levels have been associated with dedifferentiation in HCC.[6] Despite these observations, the precise role of CSRP2 in HCC progression, particularly its involvement in lenvatinib resistance, remains unclear.

In this study, we identified key genes and pathways associated with lenvatinib tolerance in HCC highlighting a mechanism involving CSRP2 and its downstream effectors. Using both in vitro and in vivo models, we demonstrate that CSRP2 reshapes the tumor microenvironment (TME) by promoting C-C motif chemokine ligand 28 (CCL28) secretion. The feasibility of targeting this mechanism to sensitive HCC to lenvatinib was further explored. Our findings uncover a novel mechanism of lenvatinib resistance, propose CSRP2 as a predictive biomarker for therapeutic response and offer a potential combination strategy to overcome drug resistance in HCC.

RESULTS

CSRP2 is a crucial marker associated with anti-lenvatinib tolerance and unfavorable prognosis in HCC

Primary liver organoids have been established as valuable models for predicting patient response to treatment, linking gene expression profiles to clinical outcomes.[9 10] To investigate the mechanisms underlying lenvatinib resistance, we analyzed HCC organoids, categorizing them into lenvatinib-resistant (n=62) and lenvatinib-sensitive groups (n=45) based on half maximal inhibitory concentration (IC50) values.[11] Differential expression analysis identified 2,484 upregulated and 2,907 downregulated genes in the lenvatinib-resistant group (|log2(fold-change)|>1, p<0.05) (figure 1A). Comparative analysis of HCC tissues (tumor diameter <2 cm, n=47) and paired non-tumorous adjacent tissues (NAT, n=47) revealed 2,087 upregulated and 1,448 downregulated genes in the tumor samples (figure 1B). Given the known *CTNNB1* mutations (S33A/S37A/T41A/S45A) commonly occur in human HCC, although these mutations alone do not induce liver cancer. *MYC* overexpression is also evident in most HCCs.[12 13] We employed hydrodynamic tail vein injections of Sleeping Beauty transposase vectors encoding *Ctnnb1* and *Myc* to model liver tumorigenesis in wild-type mice.[14] Liver samples were collected at 0, 4, 8, and 12 weeks for bulk RNA sequencing (RNA-seq) analysis (figure 1C). Results indicated dynamic changes in cell status during early (4th week), middle stage (8th week), and late stages (12th week) of tumorigenesis. Integrative analysis of HCC organoids, paired tumor samples, and mouse liver tumors identified *CSRP2, LPL, CDCA3, NKD1* and *FNDC10* as key genes (figure 1D, online supplemental figure 1A). Correlation analyses showed significant associations between *CSRP2, LPL, CDCA3*, and *FNDC10* expression and lenvatinib IC50 values, with *CSRP2* exhibiting the strongest correlation (CSRP2: R=0.57, p=6e−10; LPL: R=0.23, p=0.02; CDCA3: R=0.29, p=0.003; FNDC10: R=0.25, p=0.013; NKD1: R=0.07, p=0.48) (figure 1E, online supplemental figure 1B) and was chosen for further investigation. To further confirm the above results, biopsy samples were obtained from 40 patients who had undergone surgery after lenvatinib treatment, with tumor responses classified as resistance (n=16) or sensitive (n=24). The immunohistochemistry results revealed that patients with high CSRP2 exhibited a higher proportion of resistance cases compared with those with low CSRP2 expression (figure 1F). Moreover, immunohistochemistry (IHC) analysis of a tissue microarray (TMA) containing 107 patient samples further demonstrated that high CSRP2 expression was associated with poor prognosis (figure 1G). Univariate and multivariate analyses identified CSRP2 as an independent risk factor for predicting patient outcomes (online supplemental figure 1C). These findings suggest a strong correlation between elevated CSRP2 expression and lenvatinib resistance.

In an orthotopic xenograft model, CSRP2-overexpressing cells (Hepa1-6-*CSRP2*) exhibited a larger tumor burden compared with controls (Hepa1-6-EV) (figure 1H1). Anti-lenvatinib treatment significantly reduced tumor size in the Hepa1-6-EV group, but not in the Hepa1-6-CSRP2 group, and survival analysis revealed consistent results, indicating that CSRP2 may mediate drug resistance (figure 1J). In the cancer genome atlas liver hepatocellular carcinoma (TCGA-LIHC) cohort, CSRP2 was also significantly upregulated in HCC tissues compared with NAT tissues (online supplemental figure 1D and E). Collectively, these findings demonstrated that CSRP2 may serve as a key gene linked to lenvatinib resistance and unfavorable prognosis in HCC.

High expression of CSRP2 correlated with lenvatinib resistance and tumor progression in vitro and in vivo

Given the association between elevated CSRP2 expression and poor prognosis in patients with HCC, we further investigated the role of CSRP2 in lenvatinib resistance. We employed stable CSRP2-overexpressing HCCLM3 and CSRP2-knockout PLC/PRF/5 cell lines, selected based on their endogenous CSRP2 expression levels (online supplemental figure 2A-C). The IC50 values were quantified in HCC cell lines after CSRP2 intervention. In PLC/PRF/5 cells, CSRP2 knockdown reduced IC50 from 27.56 µM to 8.43 µM (shCSRP2#1) and 8.00 µM (shCSRP2#2), compared with the control (figure 2A). The functional consequences were further validated through quantitative colony formation assays. Under 10 µM lenvatinib treatment, empty vector (EV) control cells maintained robust colony formation capacity, while both shCSRP2 lines showed mediately reduced colony numbers (p<0.05, respectively). Additionally, our results demonstrated that cell proliferation,

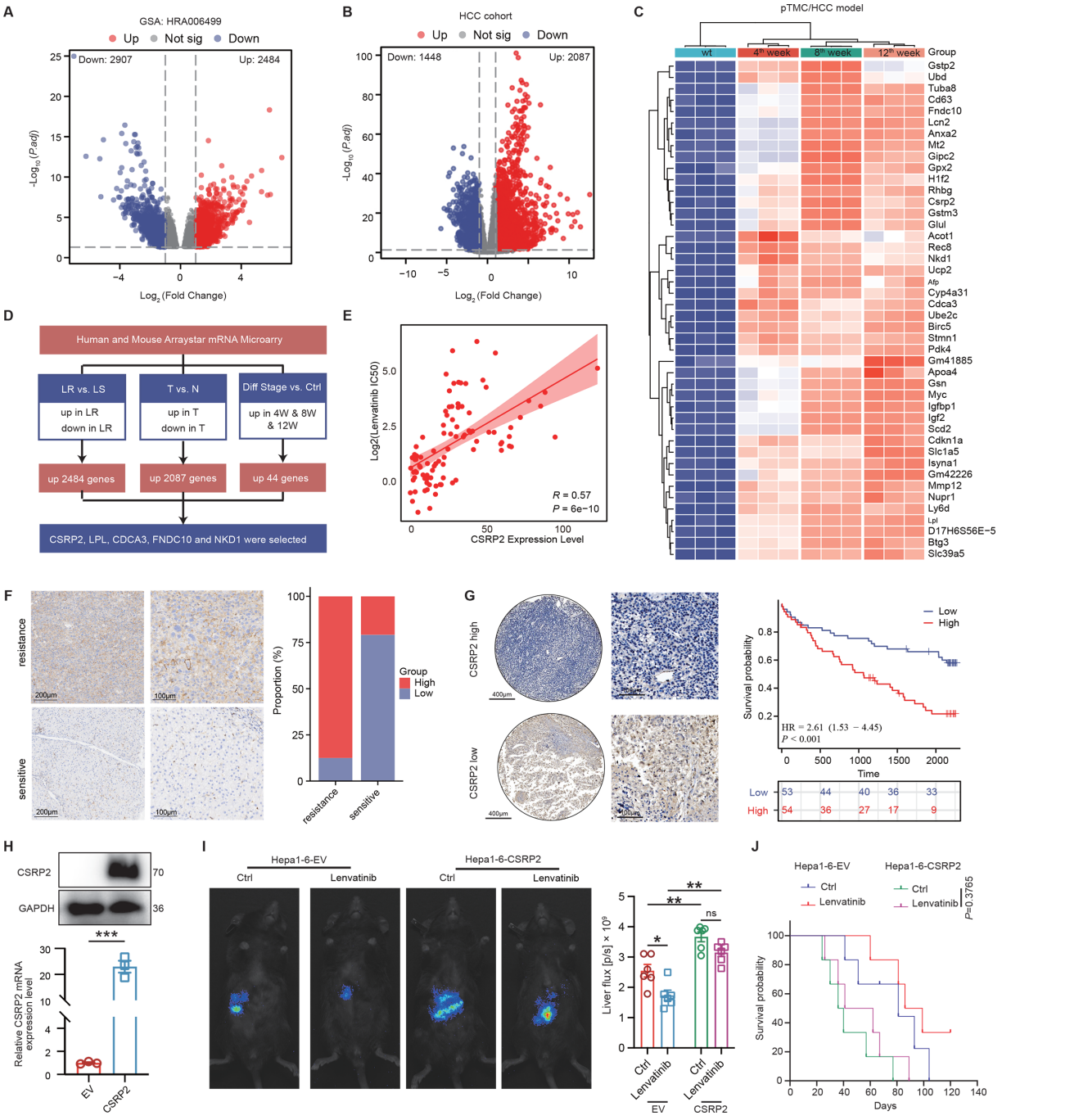

Figure 1 CSRP2 is a crucial marker associated with anti-lenvatinib tolerance and unfavorable prognosis in HCC (A). Volcano plots showing DEGs of lenvatinib-resistant and sensitive groups in HCC organoids, |log2FC|>1, p<0.05; (B). Volcano plots showing DEGs of tumor tissue and adjacent normal tissue, |log2FC|>1, p<0.05; (C). Heatmap showing the differential genes that are upregulated at different stages of tumor formation by expressing the pSB-*CTNNB1* and pSB-*Myc* using hydrodynamic tail vein injection; (D). Flow chart to identify potential genes that mediate tumor progression and lenvatinib resistance in HCC; (E). Scatterplot showing positive correlation between the level of lenvatinib resistance (represented by log2 transformed IC50 values) and mRNA expression of CSRP2 among organoids with RNA sequencing and drug testing profiles; (F). Immunohistochemistry staining of CSRP2 in HCC tissue samples from patients with sensitivity or resistance to lenvatinib therapy (left panel). The percentage of cases was analyzed by CSRP2 expression (right panel); (G). Immunohistochemistry staining of CSRP2 in tissues microarray (left panel). The OS curves analysis based on CSRP2 expression using the Kaplan-Meier method and analyzed by log-rank test (right panel); (H). Western blot and qRT-PCR assays detecting the effect of CSRP2 overexpression in Hepa1-6 cell line; (I). Bioluminescence imaging to detect tumor formation of orthotopic HCC tumors from the control and CSRP2 overexpression groups (n=6); (J). Kaplan-Meier analysis (log-rank test) of mice in each treatment group (n=6). *p<0.05; **p<0.01; ns, p>0.05. CSRP2, cysteine and glycine-rich protein 2; EV, empty vector; HCC, hepatocellular carcinoma; IC50, half maximal inhibitory concentration; mRNA, messenger RNA; OS, overall survival; qRT-PCR, quantitative reverse-transcription PCR.

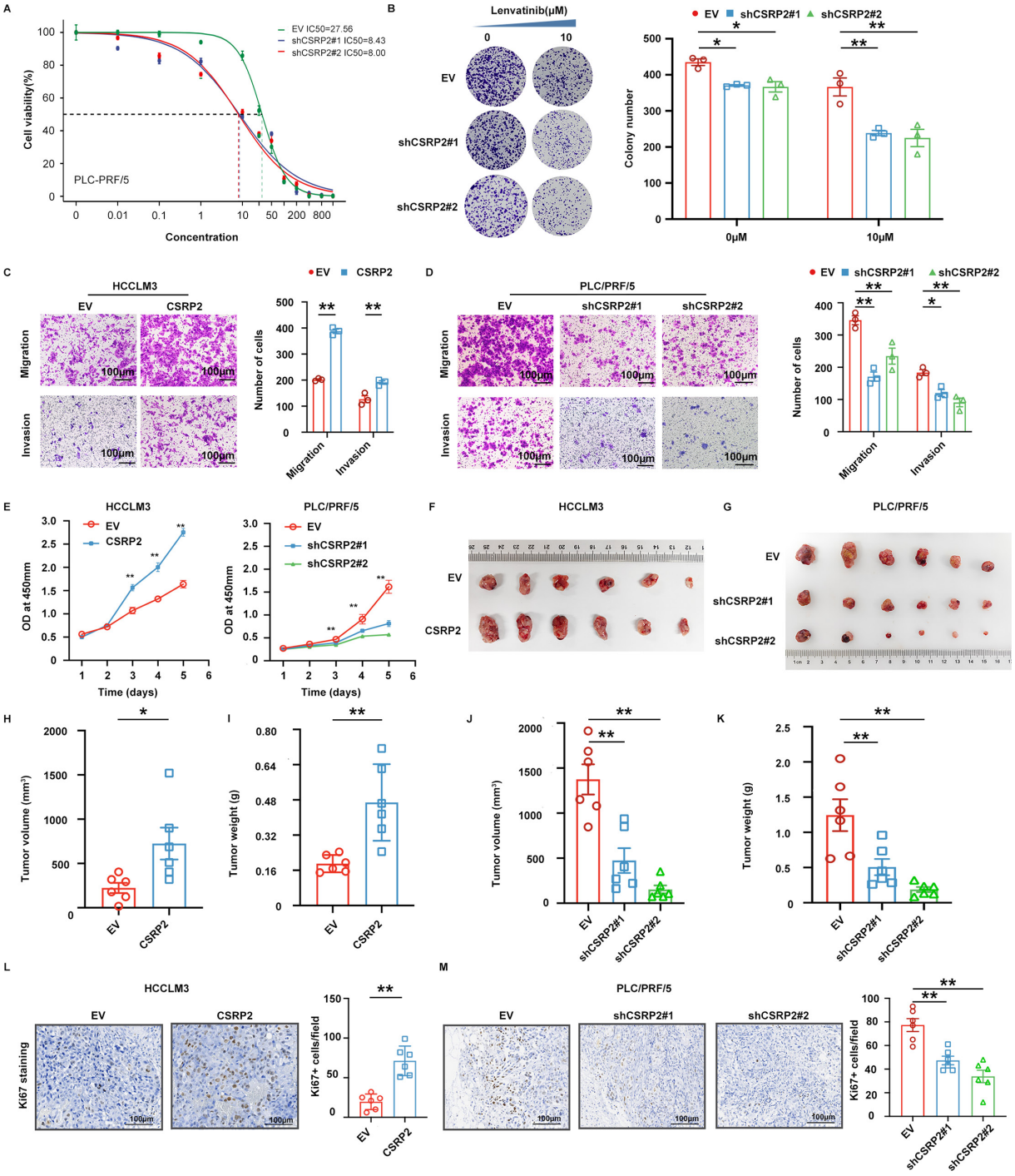

Figure 2 High expression of CSRP2 correlated with tumor progression in vitro and in vivo (A). IC50 values of lenvatinib in CSRP2-knockdown and control cell lines after treatment with the indicated concentrations of lenvatinib for 72 hours; (B). Colony formation assay of CSRP2-knockdown, and control cell lines treated with lenvatinib in 6-well dishes for 12 days (n=3). Representative images (left panel) and colony numbers (right panel) are shown; (C–D). Transwell experiments detecting the effect of CSRP2 on cell migration and invasion activity in indicated cell lines, and cell number was quantified by histogram; (E). CCK-8 experiments showing the effect of CSRP2 on cell proliferation activity in indicated cell lines; (F). Representative images of HCCLM3 subcutaneous tumors in the CSRP2 overexpression group and control group (n=6); (G). Representative images of PLC/PRF/5 subcutaneous tumors in the CSRP2 knockdown group and control group (n=6); (H–I). Using HCCLM3-CSRP2 and HCCLM3-EV cell lines to establish the subcutaneous tumor model and then tumor volume and weights were measured at the endpoint (n=6); (J–K). Using PLC-CSRP2^{low} and PLC-EV cell lines to establish the subcutaneous tumor model and then tumor volume and weights were measured at the endpoint (n=6); (L). Immunohistochemistry to detect Ki-67 expression in HCCLM3 cell lines derived-tumor model; (M). Immunohistochemistry to detect Ki-67 expression in PLC cell lines derived-tumor model. *p<0.01, **p<0.001, and ns, p>0.05. EV, empty vector; CCK-8,Cell Counting Kit (CCK-8); CSRP2, cysteine and glycine-rich protein 2; IC50, half maximal inhibitory concentration; PLC, primary liver cancer.

invasion, and migration were significantly enhanced in the CSRP2 overexpression group compared with the EV group. In contrast, these processes were markedly reduced in the CSRP2 knockdown group compared with the EV group (figure 2C–E). To further validate these findings in vivo, we subcutaneously injected HCC cells into BALB/c nude mice. The CSRP2 overexpression group exhibited significantly higher tumor weight, larger tumor size, and increased cell proliferation compared with the EV group. Conversely, the CSRP2 knockdown group exhibited lower tumor weight, reduced tumor size, and decreased proliferative activity (figure 2F–M). Collectively, these results indicate that CSRP2 plays a crucial role in promoting tumor lenvatinib resistance and progression in HCC, both in vitro and in vivo.

CSRP2 induces tumor progression and lenvatinib resistance via tumor-associated macrophages infiltration in the HCC microenvironment

Considering the essential role of the tumor immune microenvironment (TIME) in the process of treatment resistance through various mechanisms, including the mediation of immune suppression,[15 16] transcriptomic immune deconvolution was leveraged to characterize the differences in the immune context between lenvatinib-resistant and lenvatinib-sensitive groups (figure 3A). The results revealed an immune cell subset imbalance in lenvatinib-resistant tumors, characterized by CSRP2-mediated tumor-associated macrophages (TAMs) enrichment to form an immunosuppression network.

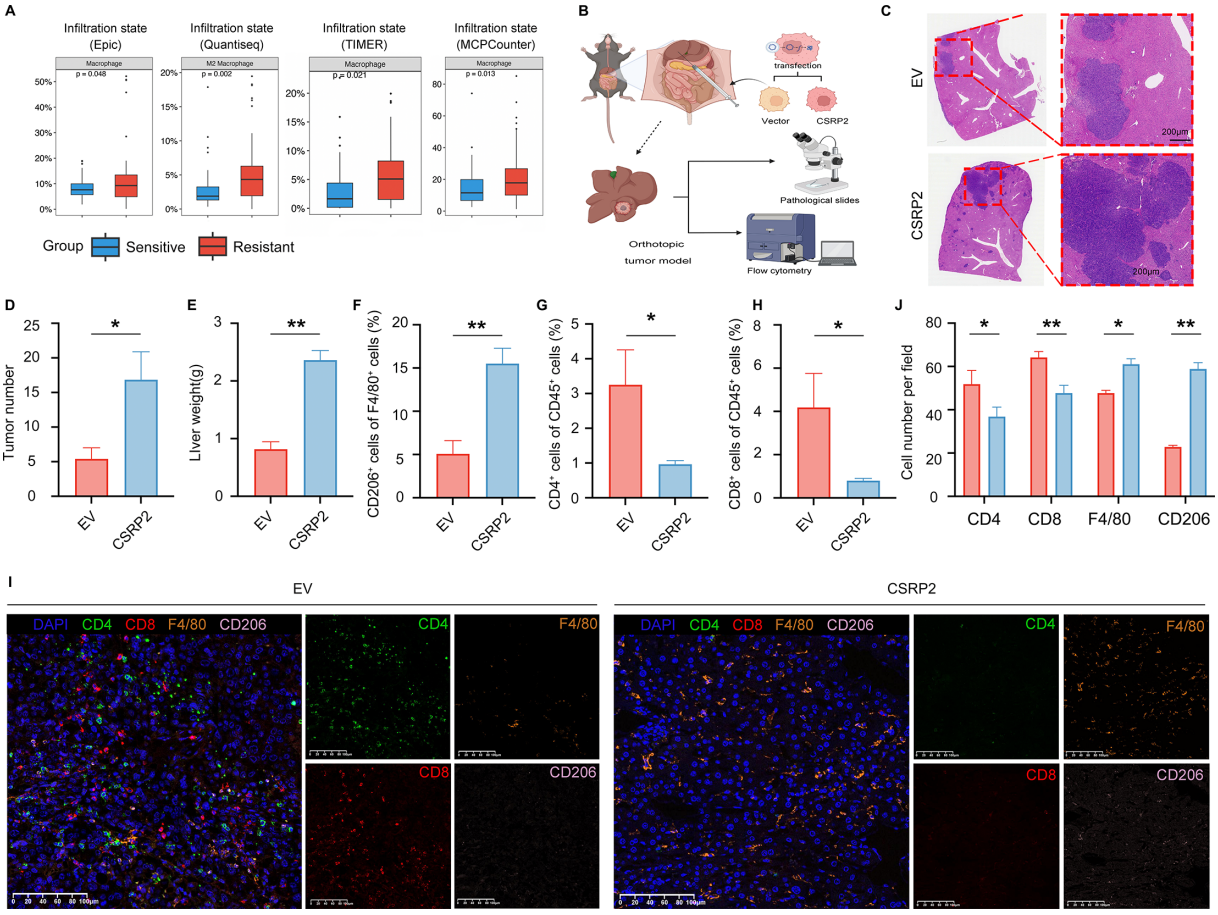

Figure 3 CSRP2 accelerates HCC progression and induces a suppressive TIME (A). Validation of tumor-associated macrophages infiltration levels among lenvatinib resistance and sensitive groups in HCC cohort; (B). Diagram of the construction model of mouse orthotopic HCC model; (C). Representative pictures of H&E staining of the orthotopic HCC tumors from the Hepa1-6-CSRP2 group and the control Hepa1-6-EV group at the end of the point (n=6); (D). The histogram showing the number of tumor nodules as indicated groups; (E). The histogram showing the average liver weight as indicated groups at the end of the point; (F). The histograms showing the percentage of $CD206^+$ cells accounting for $F4/80^+$ cells in the tumor tissue of the Hepa1-6-CSRP2 group and the control group using flow cytometry; (G–H). The histograms showing the percentage of CD4+cells and CD8+cells accounting for CD45+cells in the tumor tissue of the Hepa1-6-CSRP2 group and the control group using flow cytometry; (I–J). mIF assays verifying the infiltration of CD4+, CD8+, F4/80+ and CD206+ cells in the tumor tissue of the Hepa1-6-CSRP2 group and the control group. *p<0.01, **p<0.001, and *ns*, p>0.05. CSRP2, cysteine and glycine-rich protein 2; EV, empty vector; HCC, hepatocellular carcinoma; mIF, multicolor immunofluorescence; TIME, tumor immune microenvironment.

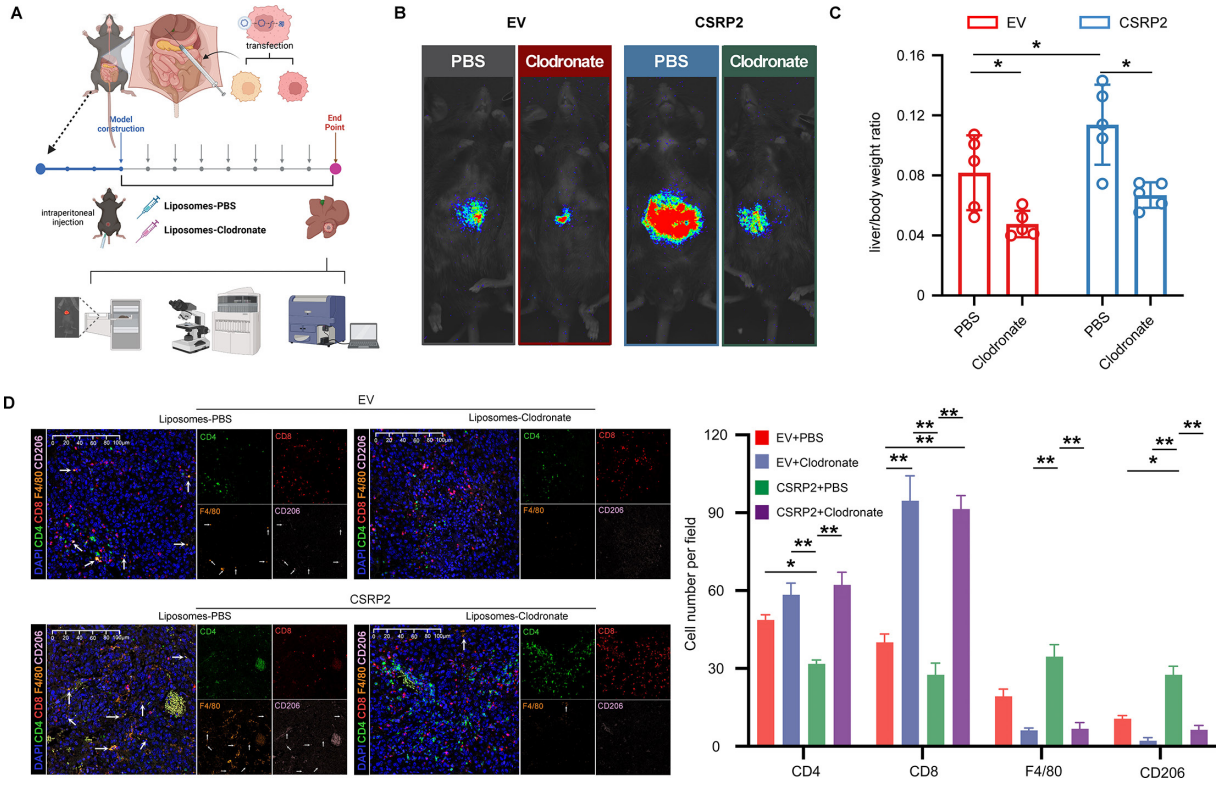

Figure 4 CSRP2 promotes tumor progression and induces a suppressive TIME that depends on the tumor-associated macrophages recruitment (A). Schematic diagram of the treatment regimen of PBS and the clodronate treatment as indicated groups; (B). Bioluminescence images of HCC tumors from the orthotopic allograft tumor model obtained at the endpoint (n=5); (C). Assessment of liver weight/body weight ratio at the end of the study (n=5); (D). mIF assays detecting the infiltration of CD4+, CD8+, F4/80+, and CD206+cells in the tumor microenvironment as indicated groups (n=5). *p<0.01, **p<0.001, and ns, p>0.05. CSRP2, cysteine and glycine-rich protein 2; EV, empty vector; HCC, hepatocellular carcinoma; mIF, multicolor immunofluorescence; PBS, phosphate-buffered saline; TIME, tumor immune microenvironment.

To further investigate the impact of CSRP2 on TIME remodeling, we constructed a tumor model by injecting *CSRP2* overexpression or control Hepa1-6 cells into mouse liver tissue. The liver tumor tissues were harvested 3 weeks post injection (figure 3B). The *CSRP2* overexpression group exhibited a higher number of tumor nodules and larger tumor sizes compared with controls (figure 3C–E). Flow cytometry analysis showed a significant increase in F4/80$^+$CD206$^+$ macrophages in CSRP2-overexpression tumors (figure 3F), accompanied by a mediated reduction in CD4$^+$ and CD8$^+$ T cells infiltration (figure 3G and H). Similar results were obtained with multiplex immunofluorescence (mIF) staining (figure 3I and J), indicating that CSRP2 drives tumor progression and resistance by inducing a suppressive TIME. Then, a TAM-depleted orthotopic allograft tumor model was used to determine if TAMs are essential for the above phenotype (figure 4A). Notably, the enhanced tumor growth observed in CSRP2 overexpressing tumors was significantly reversed following treatment with a macrophage scavenger (clodronate liposomes) compared with controls (figure 4B and C). This treatment also led to a reduction in infiltrating F4/80$^+$CD206$^+$ M2 macrophages and an increase both in CD4$^+$ and CD8$^+$ T lymphocytes, as confirmed by mIF analysis (figure 4D). These findings suggest that TAMs infiltration within the TME is crucial for CSRP2-mediated tumor progression and lenvatinib resistance.

CSRP2 promotes M2-like polarization of macrophages and low T-cell infiltration in the HCC microenvironment

Since TAMs are potent inducers of immunosuppression, we hypothesized that *CSRP2* drives immunosuppression by promoting macrophage recruitment and polarization. Thus, we differentiate THP1 cells into macrophages using phorbol-12-myristate-13-acetate (PMA) (figure 5A). Chemotactic migration assays showed that macrophages co-cultured with *CSRP2* overexpression cells exhibited significantly higher migration compared with those co-cultured with the EV group (figure 5B). Conversely, macrophage migration was reduced when co-cultured with *CSRP2* knockdown cells compared with the EV group (figure 5C), indicating that *CSRP2* overexpression in tumor cells enhances macrophage chemotaxis. We further explored the effect of *CSRP2* on macrophage polarization. Flow cytometric analysis demonstrated that the proportions of CD163$^+$ and CD206$^+$ macrophages, as well as expression levels, were significantly higher in the CSRP2 overexpression group compared with the EV group (figure 5D, online supplemental figure 3A and B). Similarly, the results were significantly reduced in the CSRP2 knockdown group compared with the EV group

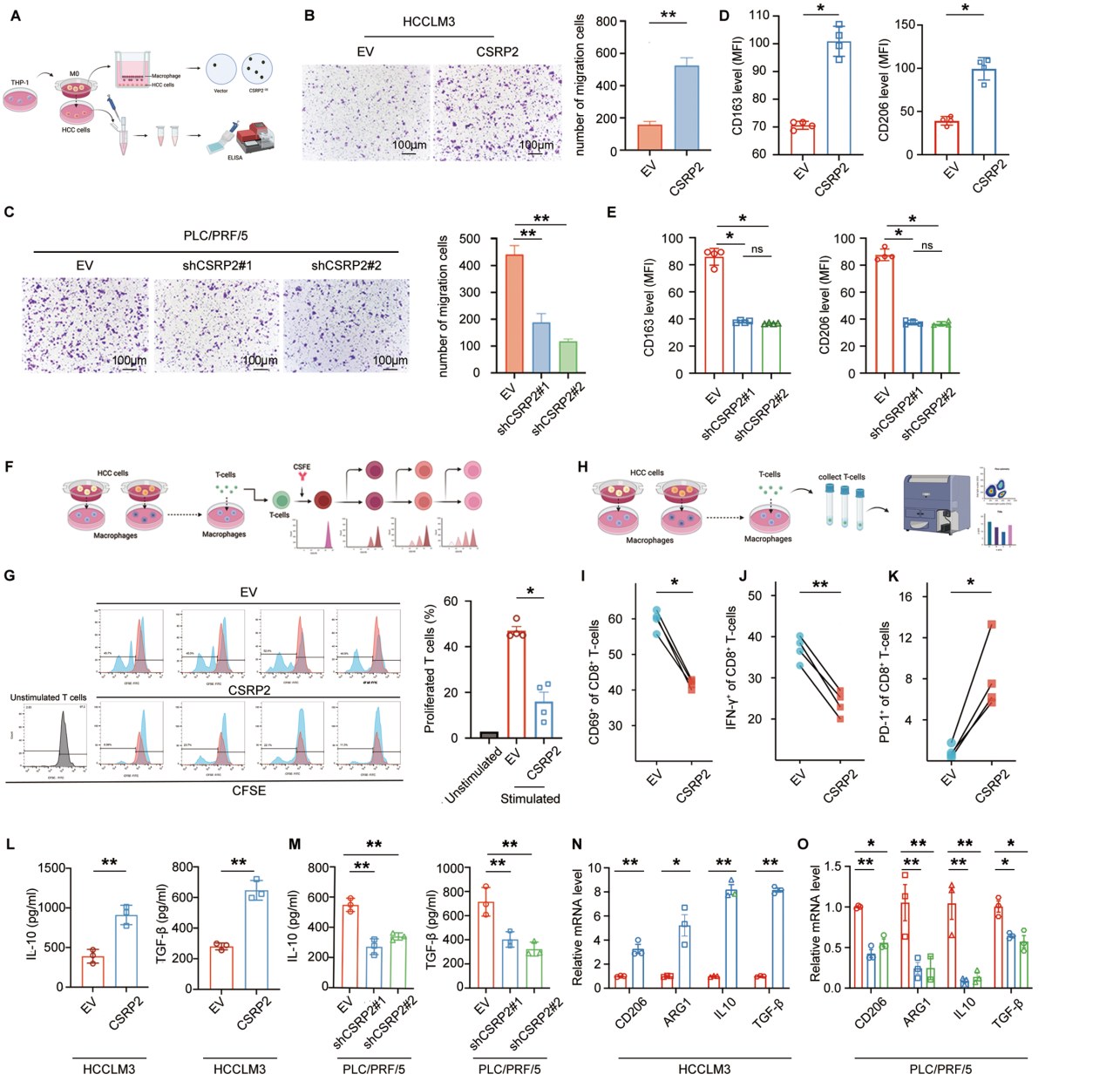

Figure 5 CSRP2 induces high TAMs infiltration and low T-cell infiltration in HCC (A). Schematic diagram of the co-culture system to explore the effects of different tumor cell culture supernatants on macrophage migration activity. The upper chamber is M0 macrophages, the lower chamber is tumor cells, and the pore size of the chamber is 8 μm; (B). Chemotactic migration assays of macrophages co-cultured with the supernatant of HCCLM3-CSRP2 and HCCLM3-EV cell lines; (C). Chemotactic migration assays of macrophages co-cultured with the supernatant of PLC-CSRP2^{low} and PLC-EV cell lines; (D). Flow cytometry showing that the expression levels of CD163 and CD206 proteins when macrophages were co-cultured with the HCCLM3-CSRP2high and HCCLM3-EV cell lines; (E). Histogram showing the CD163 and CD206 membrane protein levels in macrophages co-cultured with PLC-CSRP2^{Low} or PLC-EV cells; (F). Schematic diagram of co-culture experiments to detect the effects of macrophages derived from different tumor cells induction on T-cell proliferation; (G). CFSE assays showing the inhibition of T-cell proliferation by macrophages after treatment with the supernatant of HCCLM3-CSRP2 and HCCLM3-EV cell line; (H). Schematic diagram of T cells collected after secondary co-culture with macrophages to flow cytometry; (I–K). Flow cytometry detects the proportion of CD69$^+$ (J), IFN-γ$^+$ (K) and PD-1$^+$ (L) cells in CD8$^+$ T cells in the indicated groups; (L). Secreted IL-10 and TGF-β in the supernatants of macrophages after co-culture with HCCLM3-CSRP2 and HCCLM3-EV cell lines detected by ELISA; (M). The secretion level of IL-10 and TGF-β in the supernatant of macrophages after co-culture with PLC-CSRP2low and PLC-EV cell lines detected by ELISA; (N). qRT-PCR detected the expression level of M2 classic markers after co-cultured with HCCLM3-CSRP2-EV and HCCLM3-EV cell lines; (O). qRT-PCR detected the expression level of M2 classic markers after co-cultured with PLC-CSRP2low and PLC-EV cell lines. *p<0.01, **p<0.001, and ns, p>0.05. CSRP2, cysteine and glycine-rich protein 2; EV, empty vector; HCC, hepatocellular carcinoma; IFN, interferon; IL, interleukin; mRNA, messenger RNA; PLC, primary liver cancer; qRT-PCR, quantitative reverse-transcription PCR; TAMs, tumor-associated macrophages; CFSE, carboxy fluorescein diacetate succinimidyl ester; TGF, transforming growth factor; MFI, median fluorescence intensity.

(figure 5E, online supplemental figure 3C-F). These findings suggest that high *CSRP2* expression in liver cancer cells promotes macrophage polarization toward the M2 phenotype.

To further investigate the role of CSRP2 in the TIME, we analyzed macrophage infiltration in subcutaneous tumor models using mIF. The results showed that $CD68^{+}CD163^{+}$ M2 TAMs infiltration was significantly higher in CSRP2 overexpression subcutaneous tumors compared with controls (online supplemental figure 3G and H). In contrast, the proportion of M2 TAMs was significantly reduced in subcutaneous tumors derived from CSRP2 knockdown cells (online supplemental figure 3I and J). Moreover, macrophages co-cultured with CSRP2 overexpression tumor cells strongly suppressed T-cell proliferation (figure 5F and G) and activation (figure 5H–K, online supplemental figure 3K-N) compared with those co-cultured with CSRP2 knockdown cells or unstimulated T cells. ELISA assays revealed that macrophages co-cultured with CSRP2 overexpression HCC cells produced higher levels of interleukin (IL)-10 and transforming growth factor (TGF)-β (figure 5L and M), and quantitative reverse-transcription PCR (qRT-PCR) assays showed upregulation of CD206, IL-10, ARG1, and TGF-β mRNA expression (figure 5N and O). Collectively, these results suggest that M2 macrophages inhibit T-cell function, and CSRP2 overexpression significantly amplifies this immunosuppressive effect.

CSRP2-induced CCL28 expression contributes to macrophage polarization and recruitment in HCC

To identify the chemokines or cytokines responsible for the observed chemotactic effects, we performed RNA-seq on HCCLM3-CSRP2 cells and control HCCLM3-EV cells (figure 6A). Differential gene enrichment analysis revealed that upregulated genes were predominantly enriched in pathways related to the "cell chemotaxis" (figure 6B). Within these gene sets, CCL28 was particularly abundant compared with other candidates (figure 6C). To strengthen this finding, we expanded our analysis using a human Chemokines and Receptors PCR Array (WC-mRNA0033-H). Notably, the results showed that CCL28 maintained its position as the most significantly upregulated chemokine (1.01 vs 27.54, $p<0.0001$, (online supplemental figure 4A). In addition, correlation analyses showed significant associations between CCL28 expression and lenvatinib IC50 values ($R=0.48$, $p=4.2\times10^{-7}$) (online supplemental figure 4B). Thus, we infer that CCL28 may be one of the key transcriptional targets. Correlation analysis using the TCGA-LIHC dataset further demonstrated a significant positive correlation between CSRP2 and CCL28 expression (figure 6D). These findings were validated by qRT-PCR and ELISA assays, which confirmed elevated CCL28 levels in CSRP2-overexpressing cells. Conversely, CCL28 levels were reduced in CSRP2-knockdown cells (figure 6E and F). Further analysis using the TCGA-LIHC database revealed that CCL28 expression in liver cancer tissues was higher than in normal or adjacent non-tumorous tissues (figure 6G and H). Immunohistochemical staining of liver cancer TMA consistently showed higher CCL28 expression in tumor tissues with elevated CSRP2 expression (figure 6I). These results led us to hypothesize that elevated CCL28 secretion by tumor cells contributes to macrophage recruitment and migration in HCC, with CSRP2 playing a critical role in shaping the immunosuppressive TME by regulating TAMs infiltration.

To investigate whether CCL28 is a key effector in CSRP2-mediated processes, we conducted further experiments using transwell assay (figure 6J). As expected, the number of TAMs migration was positively correlated with CCL28 in a concentration-dependent manner (figure 6K). In the CSRP2 overexpression group, the number of migrated macrophages was significantly higher compared with the vector group. However, the enhancement of TAMs migration by CSRP2 overexpression was notably reduced by CCL28 neutralizing antibody treatment, suggesting that CSRP2 promotes macrophages migration primarily through CCL28 (figure 6L and M). Moreover, CCL28 knockdown resulted in decreased mRNA levels of CD206, ARG1, IL-10, and TGF-β (online supplemental figure 4C), as well as reduced secretion of IL-10 and TGF-β (online supplemental figure 4D and E). To further identify the receptor mediating CCL28-dependent macrophage recruitment, we performed complementary experiments using BI6901, a CCR10 inhibitor (the cognate receptor for CCL28). We observed that, in the EV group, the CCR10 inhibitor significantly decreased the macrophage migration index relative to the control. In the CSRP2 overexpression group, the CCR10 inhibitor abrogated the enhanced migration induced by CSRP2 overexpression (figure 6N), recapitulating the phenotype seen with CCL28 neutralizing antibody treatment. These data strengthen the conclusion that CSRP2-induced CCL28 expression exerts its effect on macrophage recruitment and polarization through interaction with its receptor CCR10, contributing to the formation of an immunosuppressive microenvironment in HCC.

CSRP2 cooperates with activation transcription factor 2 to regulate CCL28 transcription in HCC

Given that CSRP2 contains two LIM domains, which are key mediators of protein–protein interactions, we conducted a co-immunoprecipitation (Co-IP) assay followed by liquid chromatography-tandem mass spectrometry (LC-MS/MS) to identify proteins that interact with CSRP2 (figure 7A). Among the identified proteins, we focused on activation transcription factor 2 (ATF2), a basic/leucine zipper (bZIP) transcription factor that was highly abundant in immune complexes immunoprecipitated with CSRP2 antibodies (figure 7B). Western blot analysis further confirmed that endogenous CSRP2 was enriched in protein complexes immunoprecipitated with ATF2 antibody (figure 7C). IF analysis also demonstrated colocalization of CSRP2 and ATF2 within cells (figure 7D). Additionally, to map the

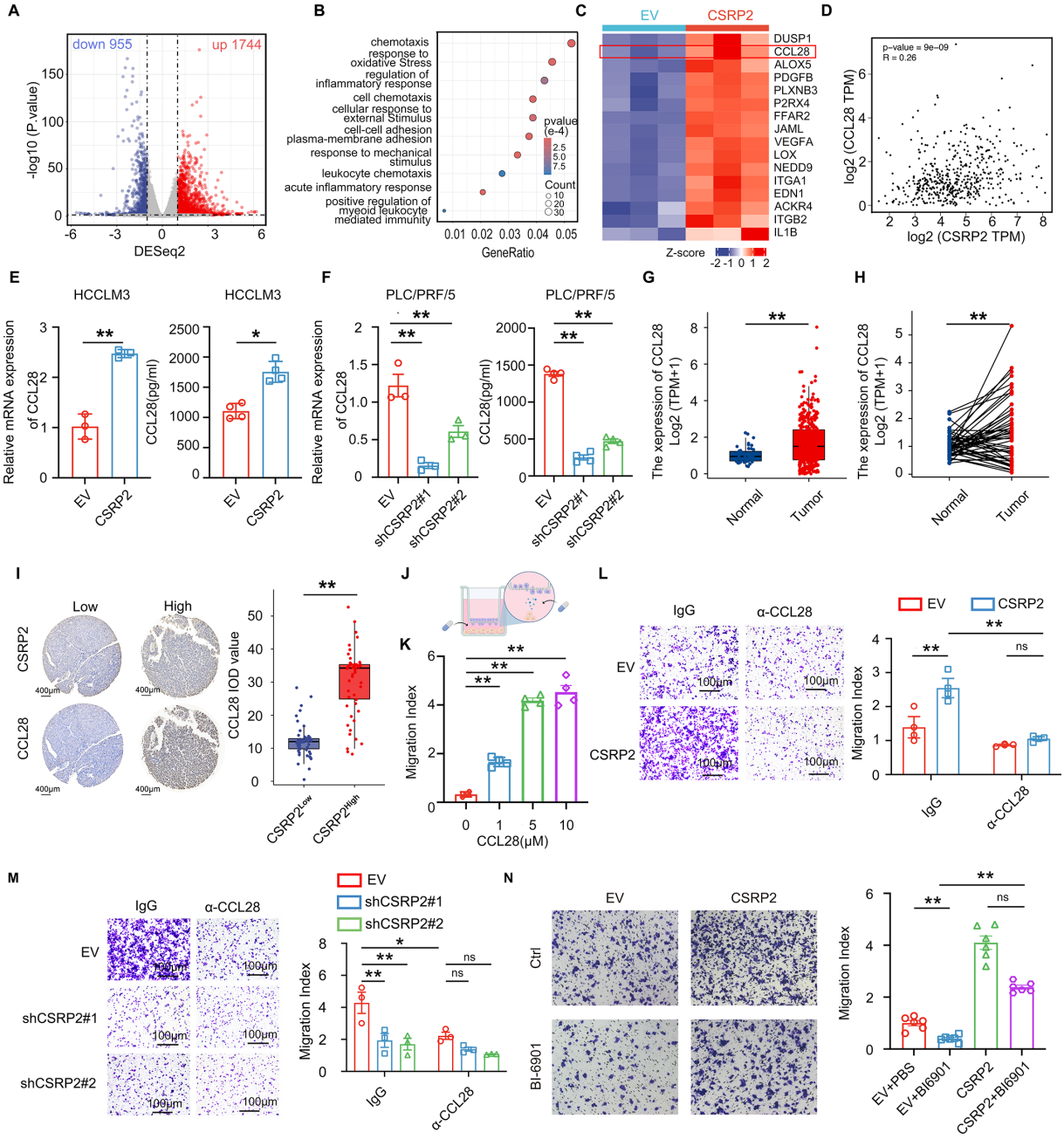

Figure 6 CSRP2-induced CCL28 expression contributes to macrophage polarization and recruitment in HCC (A). The volcano plot showing the differential expression genes between HCCLM3-CSRP2 and the control HCCLM3-EV cell lines using RNA sequencing, |log2FC|>1, p value<0.05; (B). The bubble plot showing the results of GO analysis; (C). The heatmap showing the RNA sequencing-based expression of genes in the "Chemotaxis" list in the HCCLM3-CSRP2 and the control HCCLM3-EV group; (D). Correlation analyses between CCL28 and CSRP2 were performed based on the TCGA-LIHC dataset; (E–F). Quantitative reverse-transcription PCR and ELISA assays detecting the CCL28 mRNA and secretion expression as indicated groups; (G–H). Based on the TCGA-LIHC dataset, the mRNA expression levels of CCL28 in HCC tumor tissues and adjacent tissues (left) or paired tissues (right); (I). Representative images based on CCL28 and CSRP2 IHC staining of liver cancer tissue microarray; (J). Experimental schematic diagram of the influence of the co-culture supernatant of CSRP2 stably transfected HCC cell lines on the migration ability of macrophages; (K). The effect of recombinant CCL28 protein on the migration ability of macrophages co-cultured with HCCLM3-EV cell lines; (L). The effect of CCL28 neutralizing antibody on macrophage migration ability when co-cultured with HCCLM3-CSRP2 and control HCCLM3-EV cell lines; (M). The effect of CCL28 neutralizing antibody on macrophage migration ability when co-cultured with PLC-EV and PLC-CSRP2^{low} cell lines; (N). The effect of BI6901 on macrophage migration ability when co-cultured with HCCLM3-CSRP2 and control HCCLM3-EV cell lines. *p<0.05; **p<0.01; ns, p>0.05. CCL28, C-C motif chemokine ligand 28; EV, empty vector; CSRP2, cysteine and glycine-rich protein 2; HCC, hepatocellular carcinoma; IHC, immunohistochemistry; mRNA, messenger RNA; PBS, phosphate-buffered saline; PLC, primary liver cancer; TCGA-LIHC, the cancer genome atlas liver hepatocellular carcinoma; GO, gene ontology; TPM, transcripts per million.

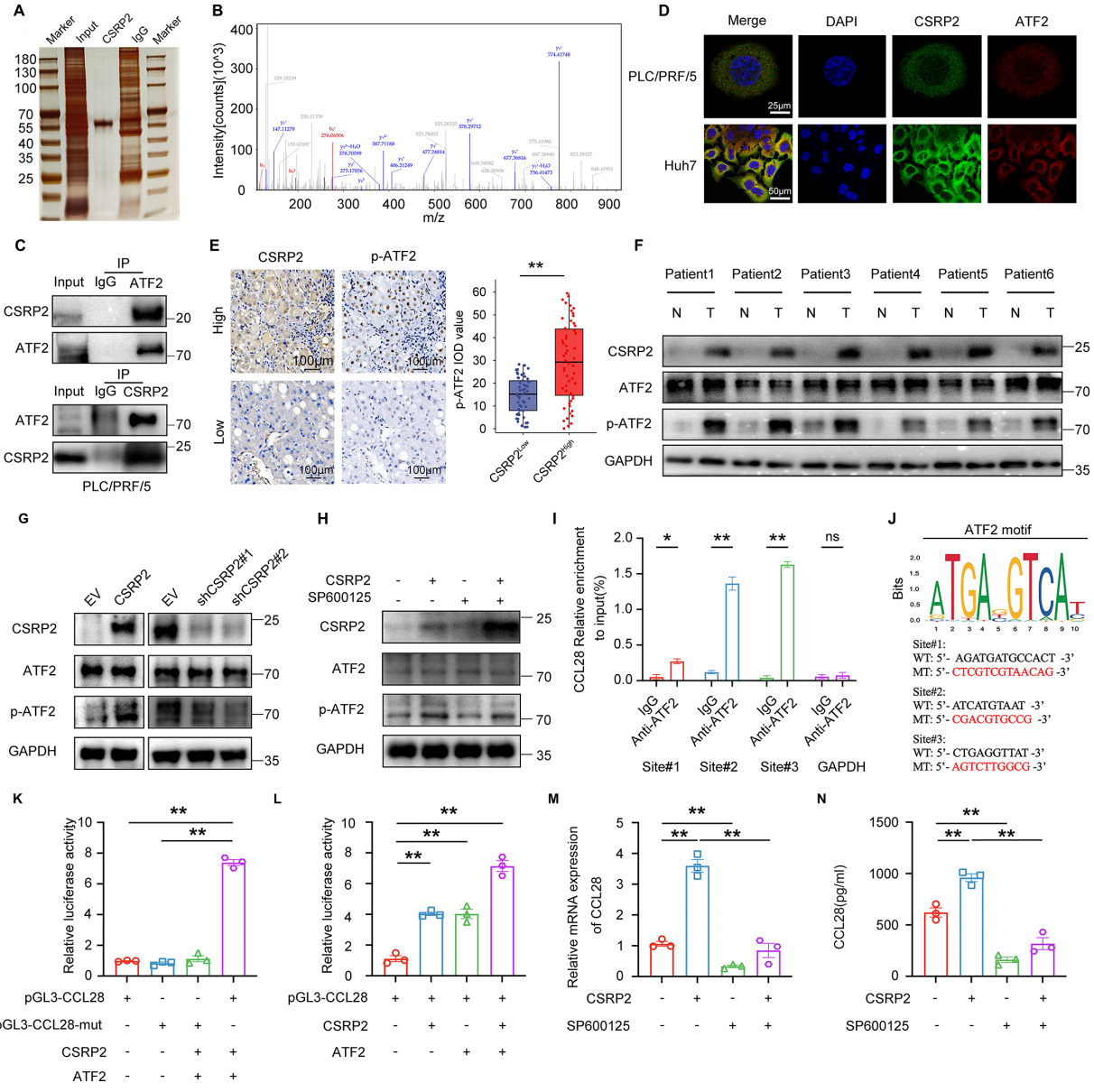

Figure 7 CSRP2 cooperates with activation transcription factor 2 (ATF2) to regulate CCL28 transcription in HCC (A). Silver staining showing the proteins bound to CSRP2 in PLC/PRF/5 cell lysate by IP assay; (B). LC-MS/MS spectrum showing the ATF2 peptides pulled down by CSRP2; (C). Co-IP of endogenous CSRP2 and ATF2 in PLC/PRF/5 cells; (D). Representative images of immunofluorescence staining showing the colocalization of CSRP2 (green) and ATF2 (red) in HCC cells. DAPI: blue; (E). Representative images of CSRP2 and p-ATF2 in TMA of HCC samples using immunohistochemical staining (left panel) and p-ATF2 expression represented as IOD values in TMA cohort (right panel); (F). Western blot verifying the expression of GAPDH, CSRP2, ATF2 and p-ATF2 in six clinical liver cancer tumor tissues and paired non-tumor tissues; (G). Western blot detecting the expression of GAPDH, CSRP2, ATF2, and p-ATF2 as indicated groups; (H). Western blot detecting the effect of JNK inhibitor SP600125 on the expression levels of CSRP2, ATF2 and p-ATF2; (I). Quantitative analysis of ChIP assay results indicating the ATF2 binding regions in the CCL28 promoter; (J–K). Dual-luciferase reporter assay showing that ATF2 and CSRP2 can enhance the transcriptional activity of the wild-type CCL28 promoter region, but has no effect on the activity of the mutant promoter region; (L). Dual-luciferase reporter assay shows that CSRP2 and ATF2 synergistically increase CCL28 promoter activity; (M–N). Quantitative reverse-transcription PCR and ELISA assays detecting the effect of JNK inhibitor SP600125 on CCL28 expression as indicated groups. *p<0.01, **p<0.001, and ns, p>0.05. ChIP, chromatin immunoprecipitation; CCL28, C-C motif chemokine ligand 28; Co-IP, coimmunoprecipitation; CSRP2, cysteine and glycine-rich protein 2; DAPI, 4',6-diamidino-2-phenylindole; EV, empty vector; GAPDH, glyceraldehyde-3-phosphate dehydrogenase; HCC, hepatocellular carcinoma; IOD, integrated optical density; LC-MS/MS, liquid chromatography-tandem mass spectrometry; p-ATF2, phosphorylated ATF2; PLC, primary liver cancer; TMA, tissue microarray.

interacting interfaces and determine the contribution of the individual LIM domains of CSRP2 to its interaction with ATF2, deletion constructs were prepared. The effective interaction was detected both with Flag-CSRP2 and the C-terminal LIM2 domain (encompassing residues 82–193). No positive enrichment was monitored

with the LIM1 domain (encompassing residues 1–81) (online supplemental figure 5A). Correlation analyses showed significant associations between ATF2 expression and lenvatinib IC50 values (R=0.53, p=1.4×10^{-8}) (online supplemental figure 5B). These results confirm the initial interaction of CSRP2 and ATF2 and reveal that LIM2 is necessary and sufficient for the interaction.

ATF2 is one of the 16 transcription factors in the Atf/Creb family that regulates normal cellular growth, development, and responses to stress.[17] It has been reported that ATF2 undergoes phosphorylation modifications, particularly at residues Thr69/71, with phosphorylation levels correlating positively with its transcriptional activity.[18] We hypothesized that phosphorylation at these sites may also play a key biological role in our study. First, we examined the correlation between CSRP2 and phosphorylated ATF2 (p-ATF2) in liver cancer TMA, confirming that p-ATF2 levels were significantly increased in tumor tissues with high CSRP2 expression (figure 7E). Similarly, CSRP2 overexpression significantly increases p-ATF2 levels, rather than total ATF2 protein abundance in six liver cancer tissues, compared with adjacent non-tumorous tissues (figure 7F). Western blot analysis showed that CSRP2 overexpression did not affect total ATF2 protein levels but significantly increased Thr69/71 phosphorylation. Conversely, reduced CSRP2 expression led to decreased phosphorylation at these sites (figure 7G). Since JNK kinase primarily mediates ATF2 phosphorylation at Thr69/71,[17] and JNK has been implicated as an upstream regulator of lenvatinib resistance,[18] we exposed HCCLM3-CSRP2 HCC cells to SP600125 (a JNK inhibitor). This treatment significantly inhibited the CSRP2-induced enhancement of ATF2 phosphorylation (figure 7H). Together, these results suggest that aberrant ATF2 expression may contribute to lenvatinib resistance in HCC.

Next, we demonstrated that ATF2 increases the activity of the CCL28 promoters, chromatin immunoprecipitation (ChIP)-quantitative PCR (qPCR) assays showed that ATF2 was significantly enriched at the CCL28 promoter compared with controls (figure 7I; Site 1, p=0.0131; Site 2, p<0.0001; Site 3, p<0.0001). Given the colocalization and functional interaction of CSRP2 and ATF2 in HCC cells, we hypothesized that CSRP2 and ATF2 might jointly interact at the CCL28 promoter. ChIP-qPCR results confirmed that CSRP2 interacts with the same binding sites as ATF2 in the CCL28 promoter region (online supplemental figure 5C); Site 1, p<0.0001; Site 2, p<0.0001; Site 3, p<0.0001). To identify the specific binding elements in the CCL28 promoter, we mutated the binding sites based on predictions from the JASPAR database (2022)[19] and the above experimental results (figure 7J). Subsequent luciferase assays revealed that mutations in the binding sites significantly reduced the positive effects of CSRP2 and ATF2 on the luciferase activity of the mutant promoter (figure 7K). Furthermore, co-transfection of ATF2 and CSRP2 significantly increased CCL28 promoter activity compared with transfection with ATF2 or CSRP2 alone (figure 7L). These findings suggest that CSRP2 enhances the binding of ATF2 to the CCL28 promoter region, thereby promoting the transcriptional activity of ATF2. Finally, we treated HCC cells with the JNK selective inhibitor SP600125 to further assess the dependence of CSRP2-induced chemokine expression on ATF2 phosphorylation. As hypothesized, SP600125 significantly reduced CCL28 mRNA and protein secretion levels (figure 7M and N). Clinically, elevated levels of CSRP2 are often accompanied by increased expression of p-ATF2 and CCL28, as demonstrated by IHC staining (online supplemental figure 6A and B). In summary, CSRP2 promotes the transcriptional expression of the downstream chemokine CCL28 through the transcriptional activation of ATF2.

Inhibitors targeting the CSRP2/ATF2/CCL28 axis sensitize lenvatinib therapy in tumor-bearing mice with high CSRP2

To investigate whether disrupting the immunosuppressive crosstalk between tumor cells and macrophages by blocking CCL28/CCR10 signaling improves the therapeutic efficacy of lenvatinib in HCC, CSRP2-overexpressing or control Hepa1-6 cells were orthotopically inoculated into the liver of wild-type C57BL/6 mice to establish the HCC model, followed by treatment with BI6901 and/or lenvatinib (figure 8A). The results showed that more significant tumor growth restriction was observed for the combination therapy than for the control and monotherapies (figure 8B–E). Moreover, as indicated by the mIF analysis, mice treated with combination therapy had more $CD4^+$ and $CD8^+$T cells and less M2-like macrophages infiltration in tumor tissues (figure 8F and G).

These results suggest that CSRP2 promotes tumor growth and lenvatinib resistance in the liver cancer microenvironment through CCL28-mediated mechanisms. Therefore, combining inhibitors targeting the CSRP2/ATF2/CCL28 pathway with lenvatinib may synergistically enhance antitumor effects, especially in patients with high CSRP2 expression.

CONCLUSION

This study identifies CSRP2 as a key driver of lenvatinib resistance in liver cancer by promoting an immunosuppressive microenvironment through TAM recruitment. Mechanistic analyses reveal that CSRP2 interacts with ATF2 via its LIM domain, facilitating JNK-dependent ATF2 phosphorylation and activating the CCL28 promoter to enhance its expression. The role of the CSRP2/ATF2/CCL28 signaling axis in lenvatinib resistance was further validated using specific inhibitors. These findings highlight the CSRP2/ATF2/CCL28 axis as a potential biomarker for predicting liver cancer progression and lenvatinib resistance, while offering a promising target for combination therapies to improve outcomes in patients with HCC.

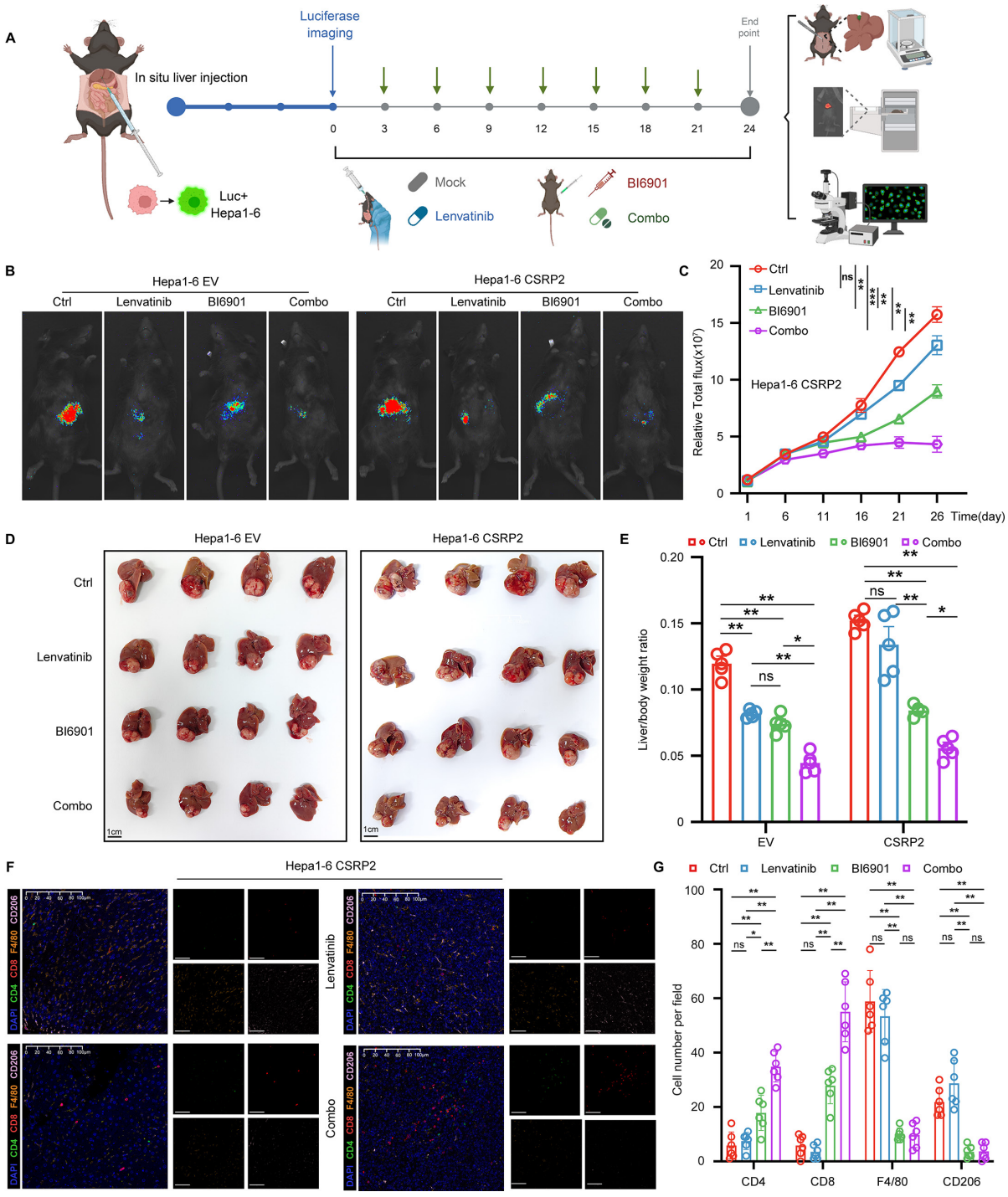

Figure 8 The inhibitors sensitize lenvatinib therapy in tumor-bearing mice with high CSRP2 expression by targeting the CSRP2/activating transcription factor 2/C-C motif chemokine ligand 28 axis (A). An HCC orthotopic allograft tumor model was constructed in C57BL/6 mice. Mice were treated with a mock or CCR10 inhibitor, BI-6901. Bioluminescence images of HCC tumors from the orthotopic allograft tumor model were monitored every 5 days (n=4); (B–E). Representative bioluminescence images (B), dynamic curve of bioluminescence signal value (C), gross appearance of the orthotopic HCC tumors from the indicated treatment groups (D), liver/body weight ratios (%) (E) are shown; (F). Representative mIF images showing CD4 (green), CD8 (red), F4/80 (yellow), and CD206 (pink) in Hepa1-6-CSRP2 xenograft HCC tissues from indicated groups; (G). Quantification of corresponding immune cells by mIF analysis. *p<0.01, **p<0.001, and ns, p>0.05. CSRP2, cysteine and glycine-rich protein 2; EV, empty vector; HCC, hepatocellular carcinoma; mIF, multiplex immunofluorescence; TAMs, tumor-associated macrophages.

DISCUSSION

This study reveals that CSRP2 induces the formation of an immunosuppressive microenvironment in HCC through TAMs recruitment, thereby mediating resistance to lenvatinib treatment. We initially screened datasets comprising 107 organoids from patients with HCC and

identified CSRP2 as a candidate gene potentially involved in lenvatinib resistance. Our findings further indicate that CSRP2 overexpression exerts a protumorigenic effect by promoting intratumoral macrophage recruitment and M2-like polarization, which leads to an immunosuppressive microenvironment. Altogether, CSRP2 not only shapes an immunosuppressive microenvironment by recruiting M2 macrophages but also directly regulates tumor cell migration, invasion, and proliferation, demonstrating its dual protumor roles. Mechanistically, we demonstrated that CSRP2 binds to ATF2 through its LIM domain and promotes JNK-dependent ATF2 phosphorylation, thereby upregulating CCL28 expression by activating its promoter. Finally, we illustrated the involvement of the CSRP2/ATF2/CCL28 signaling axis in mediating lenvatinib resistance using specific inhibitors. The CSRP2/ATF2/CCL28 signaling axis is anticipated to serve as a predictor of malignant progression in HCC and resistance to lenvatinib treatment, providing a new direction for drug screening and combination therapy in HCC.

Despite advances in liver cancer research and clinical diagnosis and treatment technologies, the overall prognosis for patients with liver cancer remains unsatisfactory.[20] Targeted therapies, such as lenvatinib, have become crucial in systemic treatment; however, treatment resistance driven by factors like genetic instability, driver mutations, or abnormalities in signal transduction pathways significantly limits their efficacy. Understanding the mechanisms of drug resistance and developing interventions to enhance the effectiveness of targeted therapies for liver cancer is an urgent challenge for clinicians.

Using multisource datasets, we identified CSRP2 as a potential target associated with lenvatinib resistance. CSRP2, a member of the CSRP family, encodes a group of short LIM domain proteins (21 kDa) and plays a key role in development and differentiation.[4] Functional analyses show that CSRP2 promotes B-cell acutelymphoblastic leukemia (ALL) cell proliferation and migration, supporting the notion that tumor hypoxia is a key determinant of CSRP2 upregulation in breast cancer. Survival analyses indicate that CSRP2 overexpression is associated with significantly shorter recurrence-free and overall survival (OS).[5] Beyond breast cancer, CSRP2 has been identified as a downstream target of H19, a long non-coding RNA linked to survival in patients with colorectal cancer.[21] Patients with high CSRP2 expression in colorectal tumors have significantly shorter OS, and a combined analysis of H19 and CSRP2 appears to be a strong predictor of OS. Therefore, the specific role of CSRP2 in tumor development may vary depending on the tumor type. There are limited studies on CSRP2 in liver cancer, and none have reported its role in mediating treatment resistance.

Our study, both in vivo and in vitro, indicates that high CSRP2 expression promotes the malignant phenotype of liver cancer and affects the therapeutic efficacy of lenvatinib. Based on the transcriptomic data on HCCLM3 cells with CSRP2 overexpression and their controls, gene set enrichment analysis (GSEA) analysis revealed that elevated CSRP2 activates the PI3K-Akt pathway and the degradation of the extracellular matrix (eg, activation of matrix metalloproteinases) (online supplemental figure 7A and B). Collectively, these findings indicate that CSRP2 significantly promotes tumor growth and confers resistance to lenvatinib in HCC, potentially through the modulation of the indicated pathway.

The TIME significantly impacts tumor progression, invasion and metastasis. To reflect real-world conditions, we established an orthotopic liver cancer model in immune-competent mice to verify the role of CSRP2. We found that CSRP2 promotes in situ liver cancer growth and induces resistance to lenvatinib treatment. Taken together, these results indicate that CSRP2 promotes liver cancer progression and participates in lenvatinib resistance. Notably, we reanalyzed the dataset derived from the HCC organoids revealed that high CSRP2 expression correlates with elevated IC50 values for sorafenib, regorafenib, and apatinib, suggesting a potential broader role in tyrosine kinase inhibitors (TKI) resistance. However, the lack of universal significance in group comparisons underscores the complexity of resistance mechanisms, which may involve drug-specific pathways alongside shared axis like CSRP2/ATF2/CCL28 (online supplemental figure 8). Future studies using in vitro and in vivo models will be essential to dissect these relationships mechanistically and explore the potential clinical applications to overcome TKI resistance. Tumor treatment resistance involves both intrinsic and extrinsic factors. Intrinsic factors refer to genetic or epigenetic changes in tumor cells that produce heterogeneity, leading to treatment resistance through clonal expansion under survival pressure selection. This includes enhanced drug efflux, weakened apoptosis signals, and metabolic reprogramming.[22 23] Extrinsic factors mainly involve the TME, a complex system of interactions between cells, signaling molecules and matrix structures within tumor tissue. Intrinsic and extrinsic factors interact and promote each other, driving tumor occurrence, progression, metastasis, and even regulating treatment responses.[22] Lenvatinib inhibits tumor angiogenesis and triggers changes in the immune microenvironment, possessing certain immune regulatory functions. The combination of lenvatinib and immune checkpoint inhibitors significantly improves efficacy in liver cancer, indicating that its effectiveness is related to the TME, especially immune factors.[24] It can be speculated that the complex network formed by interactions between cell populations in the TME can limit T-cell function through multiple mechanisms, reducing the effect of lenvatinib treatment and leading to drug resistance. Therefore, in studying the mechanism of resistance to lenvatinib caused by CSRP2, we focused on the immune microenvironment of liver cancer, particularly the influence of immune factors.

We constructed a mouse liver cancer model by directly injecting liver cancer cells into the liver. Using flow cytometry and multicolor IF, we found that CSRP2

overexpression caused a significant increase in tumor-infiltrating macrophages, mainly of the M2 type. Depleting TAMs through drug treatment reversed the effects of CSRP2 overexpression on tumor growth and $CD8^+$ T-cell changes. Additionally, we demonstrated through an in vitro co-culture system that CSRP2 overexpression enhances the chemotaxis of liver cancer cells to macrophages and further affects the proliferation and function of $CD8^+$ T cells. Finally, we verified the correlation between high CSRP2 expression, TAMs infiltration, and reduced $CD8^+$ T cells in TMA through multiplex immunohistochemistry(mIHC). These results suggest that upregulated CSRP2 in HCC reshapes the TIME by recruiting macrophages and promoting M2 polarization, leading to reduced $CD8^+$ T-cell numbers and functional inhibition, transforming the TME toward immunosuppression and promoting tumor progression. To our knowledge, no previous studies have investigated the relationship between CSRP2 and the tumor TME. Our findings link CSRP2 to the TME for the first time, suggesting that its overexpression reshapes the TME toward immunosuppression by recruiting TAMs and promoting M2 polarization.

Previous studies have extensively reported that TAMs can induce tumor immunosuppression by expressing immune checkpoint molecules, secreting inhibitory inflammatory factors, and recruiting suppressive immune cells such as regulatory T cells (Tregs), thereby inhibiting the infiltration and activation of effector T cells.[25] Therefore, we hypothesized that CSRP2 overexpression in HCC may induce the recruitment and polarization of TAMs through a mediator, shaping the immunosuppressive microenvironment in liver cancer. We found that CSRP2 in tumor cells induces macrophage chemotaxis, migration and polarization by upregulating CCL28 secretion. Using a CCL28 neutralizing antibody in an in vitro co-culture system, we confirmed its impact on TAMs behavior and function in HCC. The results showed that the CCL28 neutralizing antibody significantly reduced TAMs chemotaxis and polarization induced by CSRP2 overexpression. These findings suggest that CSRP2-mediated CCL28 expression increases TAMs infiltration in HCC, thereby reducing the infiltration and activation of antitumor immune cells in the microenvironment.

ATF2 is 1 of the 16 Atf/Creb family transcription factors. The different transcriptional functions of ATF2 are attributed to its homodimerization or heterodimerization with other AP-1 transcription factors through the bZIP domain and its phosphorylation at residues 69/71 by the stress kinase JNK or p38.[26] As a stress-inducible transcription factor, ATF2 regulates gene expression programs related to cell cycle control, cytokine expression, and cell death.[17] We first verified that CSRP2 interacts with ATF2 through IF and Co-IP experiments. CSRP2 promotes the serine phosphorylation of ATF2 at positions 69/71 through JNK, thereby enhancing the transcriptional activity of ATF2. Based on these observations, we hypothesized that CSRP2 regulation of CCL28 expression may depend on ATF2 transcriptional activity. Using ChIP-qPCR experiments, we found that ATF2 directly binds to the promoter region of CCL28. Fluorescent reporter gene experiments showed that mutating the binding site affected transcriptional activity. Co-transfection of CSRP2 and ATF2 significantly enhanced the transcriptional regulatory activity of the CCL28 promoter region compared with transfection of ATF2 or CSRP2 alone. Finally, using a nude mouse subcutaneous transplantation tumor model and an orthotopic tumor cell injection tumor model, we verified that the abnormal activation of the CSRP2/ATF2/CCL28 signaling axis is related to lenvatinib resistance. Pathway inhibitors such as SP600125 and BI6901 can be considered candidate drugs for combination therapy with lenvatinib. However, the specific mechanism by which CSRP2, with its dual LIM domains, binds to ATF2 still requires further exploration in further studies. In the future, more paired samples will be collected to deeply explore the dynamic evolution of the CSRP2/ATF2/CCL28 axis in drug resistance, so as to strengthen the clinical relevance and translational significance of the research results.

MATERIALS AND METHODS

Patients with HCC and tissue specimens

This study included 154 patients with HCC from two independent cohorts. Cohort 1, consisting of 47 patients, was used for RNA-seq. Cohort 2 included 107 patients with paraffin-embedded tissue samples for TMA and IHC analysis, all of whom underwent curative resections in 2010 and were followed-up until June 13, 2016. Curative resection was defined as complete tumor removal with histologically confirmed cancer-free margins. Patients were excluded if they underwent palliative surgery, had prior interventions (eg, transhepatic artery embolization, chemotherapy, or radiotherapy), or were diagnosed with other primary malignancies or inflammatory diseases during follow-up. HCC diagnoses were confirmed histopathologically following WHO criteria. Postoperative monitoring occurred every 3–6 months, as previously described.[27] OS was measured from the date of surgery to death or last follow-up. In addition, a total of 40 surgical samples were collected from patients with HCC treated with lenvatinib. The tumor response was evaluated by abdominal contrast-enhanced MRI or CT based on the Response Evaluation Criteria in Solid Tumors V.1.1. Patients with a partial response were classified as lenvatinib-sensitive, whereas those with stable disease or progressive disease were classified as clinically resistant to lenvatinib.

Mouse tumor model and treatments

A mouse liver tumor orthotopic transplantation model was established using the mouse HCC cell line Hepa1-6 as previously described.[28] Briefly, 6-week-old C57BL/6 mice were anesthetized and injected in the subcapsular region of the liver with 20 µL of cell/Matrigel solution

(containing 5×10^5 Hepa1-6 cells) using a syringe with a 33 G needle. After surgery, mice were incubated at 25°C until awakening. To the endpoint, orthotopic tumors were excised, fixed, weighed, and embedded in paraffin, followed by H&E staining. Tumor sites were calculated as the number of tumor nodules per field of view. A subcutaneous tumor transplantation model was established using HCCLM3 or PLC/PRF/5 cells. A total of 5×10^6 cells were injected subcutaneously into 6-week-old nude mice. Lenvatinib or SP600125 treatment was executed when the tumor size reached~6 mm×6 mm (length×width)[29] as indicated in the related figures. As described in a previous study, complementary DNA (cDNA) of mouse Myc gene was cloned into the transposon vector through the MluI and SpeI restriction enzyme sites, obtaining the pT3-Neo-EF1a-Myc plasmid. Next, mutated forms of mouse Ctnnb1 (Δ90Ctnnb1) was generated by PCR cloning of mouse Ctnnb1 cDNA. Then, the Myc and Δ90Ctnnb1 transposon plasmid (pT3-EF1a-Myc-Δ90Ctnnb1, pTMC) was generated through the AscI and NotI restriction sites. For construction of the pTMC-luciferase plasmid (pTMC-Luc), the luciferase fragment was linked to Myc by P2A using In-Fusion cloning. For HDTV, a 30 µg DNA mixture, comprising transposon and transposase-encoding plasmid in a 5:1 ratio, was suspended in a 0.9% saline solution. The final injection volume was adjusted to 10% of the mouse's body weight and administered via tail vein within 5–7 s.[30] All mice were maintained on a 12/12 hours day/night cycle and allowed free access to food and water. We strictly adhered to animal care principles and ethics and received approval from the Institutional Animal Care and Use Committee of the Shanghai Model Organisms Center (No. 2022–0051).

Tumor-infiltrating immune cell isolation and flow cytometry

Fresh tissue was perfused using cold phosphate-buffered saline (PBS), dissociated with 2 mg/mL collagenase (Sigma, #C5138) and 1×DNase I (Roche, #11284932001) in Roswell Park Memorial Institute (RPMI)-1640 medium at 37°C for 30 min, and then filtered through a 70 µm strainer. The suspended cells were centrifuged at 800 g for 5 min. After removing the supernatant, the cell pellet was collected. $CD8^+$ T cells were isolated using anti-CD8 magnetic beads (STEMCELL, 17853), followed by macrophage cells using anti-CD14 magnetic beads (STEMCELL, 19359). After separation, the cells are resuspended in the corresponding immune cell culture medium for subsequent experimental operations or culture. For antibody staining, the cell pellet was resuspended in 200 µL PBS+2% fetal bovine serum (FBS) solution. Before staining, single-cell suspensions were blocked with anti-mouse CD16/CD32 antibodies (BD Pharmingen, #553141) for 15 min. Then, the fluorophore-conjugated antibody mixture was added and stained on ice for 30 min in the dark. The flow cytometry antibodies used in this study were anti-mouse CD3-PerCP-Cy5.5 (BD Pharmingen, #551163), anti-mouse CD4-FITC (BD Pharmingen, #557307), anti-mouse CD8- PE-CY7 (BD Pharmingen, #552877), anti-mouse CD25-BV421 (BD Pharmingen, #564370), anti-mouse PD-L1-APC(BD Pharmingen, #564715), anti-Human CD163-PE (BD Pharmingen, #556018), anti-Human CD206-APC (BD Pharmingen, #55088), anti-Human CD69-PE (BD Pharmingen, #560738), anti-Human PD1-BV605 (BD Pharmingen, #563245), anti-Human IFN-γ-PerCP-Cy5.5 (BD Pharmingen, #560704) and anti-Human CCR7-BV605 (BD Pharmingen, #563711). Flow cytometry analysis was then performed using BD FACSAria III. FlowJo V.10.4.2 was used for further analysis.

RNA sequencing

RNA-seq libraries were constructed using the NovaSeq 6000 sequencer (Illumina). The quality of sequencing reads was evaluated using FastQC. Adaptor sequences and low-quality score bases were trimmed using Trimmomatic (V.0.36). These reads were then mapped to the human genome reference GRCh38 from Ensembl release 98 using STAR (V.2.5.2b). Differentially expressed genes (DEGs) were analyzed using the DESeq2 (V.1.42.0) R package. Pathway analysis was performed using the software clusterProfiler (V.4.10.0), and the plot was generated using ggplot2 (V.3.4.4) in R.

Chemotaxis experiment

Different groups of tumor cells (5×10^5) were placed in the bottom chamber of a 6-well plate. The differentiated THP-1 cells or purified $CD14^+$ macrophage cells (2×10^5) were placed into the top insert of a Transwell and cultured in macrophage differentiation medium containing 100 ng/mL macrophagecolony stimulating factor (M-CSF) (STEMCELL, 78059). After 48 hours, macrophages that migrated and adhered to the lower surface of the Transwell membrane were fixed with 4% paraformaldehyde and stained with 1% crystal violet, and the number of migrated macrophages was counted by ImageJ.

CCK-8 proliferation assay

The cell counting kit-8 (CCK-8) assay was performed to measure capacity for cellular proliferation. Briefly, 1,000 cells were seeded into a 96-well flat-bottomed plate. At each time point, the plate was added CCK-8 to the medium and incubated for 2 hours at 37°C, and the optical density was measured at 450 nm using a multimode microplate reader (Thermo Fisher Scientific, Waltham, Massachusetts, USA).

Transwell assays

For the Transwell migration assay, appropriate amounts of cells were incubated in the upper compartment of the chamber. After 48 hours incubation at 37°C with 5% CO_2, cells passing through the chamber were fixed with 4% paraformaldehyde at room temperature for 30 min and stained with 0.1% crystal violet at room temperature for 10 min. The number of cells invading through the chamber was counted using a microscope (Olympus, Japan).

Immunohistochemistry staining

HCC tissue microarray was heated at 60°C for 1 hour. After dewaxing, rehydration and antigen retrieval, non-specific background staining was blocked with 5% Bovine Serum Albumin (BSA) and incubated with corresponding primary antibodies diluted in Antibody Diluent (NCM Biotech, Suzhou, China) overnight at 4°C, then incubated with horseradish peroxidase (HRP)-conjugated secondary antibodies at 37°C for 1 hour. DAB Substrate Kit (GenTech, Shanghai, China) was used to control the degree of chromogenic reaction. Tissue sections were then incubated with hematoxylin for nuclear counterstaining. Stained sections were scanned using the standard microscope (Olympus, Japan) or the CaseViewer software (3DHISTECH, Budapest, Hungary). Then, loading the scanned clear histochemical pictures into the QuPath software (V.0.5.1), according to its official guidance, set the parameters and obtain various types of data including staining intensity, positive cell proportion or count and H-score. The results were then rechecked independently by two pathologists and disagreements were resolved by reaching a consensus.

ChIP assay

The ChIP assay was performed using the SimpleChIP Enzymatic Chromatin IP Kit (CST, USA) according to the manufacturer's protocol. After ultrasonication, equal aliquots of chromatin sample were immunoprecipitated with anti-*ATF2* (Abcam, #ab32160), anti-*CSRP2* (#10892–2-AP, Proteintech, USA), or IgG at 4°C overnight in rotation. The purified DNA was analyzed using reverse-transcription-qPCR, and the relative expression of 2% input was calculated to assess DNA enrichment within the immunocomplex. Primers were listed in the Supporting Information.

Luciferase reporter assay

CCL28 promoter regions, spanning from −2,000 to +250 of the transcription start site, were amplified from genomic DNA and cloned into the pGL3-Basic vector (Genomeditech Biotech, China). These promoter luciferase reporters were then cotransfected with renilla luciferase expression plasmid using lipofectamine 3000 reagent (Invitrogen, California, USA). 48 hours later, the firefly and renilla luciferase activities were measured using the Dual-Luciferase Kit (Promega, France) according to the manufacturer's instructions.

Co-IP and LC-MS/MS

The cells were lysed using NP-40 lysis buffer (Beyotime, #P0013F) supplemented with protease and phosphatase inhibitor cocktails, followed by an incubation with primary antibody in rotation at 4°C overnight. Protein A/G-magnetic beads (MedChemExpress, #HY-K0202) were then added to the lysates for 2 hours at room temperature. The beads were collected using a magnetic stand and washed three times. The bound proteins were subjected to analysis using mass spectrometry. Briefly, the proteins described above were resolved on 10% sodium dodecyl sulfate polyacrylamide gel electrophoresis (SDS-PAGE) gels and visualized by Coomassie blue staining (Beyotime, #P0003S). Then, the extracted proteins were mixed with matrix and spotted on a sample plate. The masses of peptides were identified by time of flight (ABI 4700 protein analyzer, ABI). MS data were searched against the Swiss-Prot database of Homo sapiens.

PCR array analysis

To dissect the mechanism that underlies the effect of CSRP2 on macrophages, we analyzed the cytokine profiles of supernatants from control and CSRP2 overexpression HCC cells using the human Chemokines and Receptors PCR Array (Wcgene Biotech, Shanghai, China) following the manufacturer's protocol.

Lenvatinib cytotoxicity assay

Lenvatinib cytotoxicity was assessed using the CCK-8 assay in HCC cell lines. Cells were seeded at 2×10ˆ3 cells per well in a 96-well plate and treated with increasing concentrations of lenvatinib (ranging from 0.01 µM to 750 µM) for 72 hours. Cell viability was determined by the CCK-8 assay according to the manufacturer's protocol. The IC50 value was calculated by plotting the percentage of cell viability against the concentration of lenvatinib and fitting the data to a four-parameter logistic dose-response curve using GraphPad Prism.

Statistical analysis

GraphPad Prism V.9.0 software was used to analyze the experimental data. Each experiment was independently repeated at least three times, and the results are represented as the means±SD or means±SEM. Comparisons were analyzed using an unpaired two-tailed Student's t-test or one-way analysis of variance. Paired two-tailed Student's t-tests were used to compare tumors and adjacent tissues. The p values are indicated in the related figures; *p<0.01, **p<0.001, and ns, p>0.05.

Author affiliations

[1]Department of Hepatobiliary Surgery and Transplantation, Liver Cancer Institute, Zhongshan Hospital, Fudan University, Shanghai, Shanghai, China
[2]Key Laboratory of Carcinogenesis and Cancer Invasion (Fudan University), Ministry of Education, Zhongshan Hospital, Fudan University, Shanghai, Shanghai, China
[3]Department of Gynecologic Oncology, Cancer Center, Zhongshan Hospital, Fudan University, Shanghai, China
[4]Department of Colorectal Surgery, Zhejiang University School of Medicine, Hangzhou, China
[5]Department of Thoracic Surgery, Shanghai Jiao Tong University School of Medicine, Shanghai, China
[6]Clinical Center for Biotherapy, Zhongshan Hospital, Fudan University, Shanghai, Shanghai, China

Contributors XH and ZH designed the experiments. CC, SS, PW and XY performed and analyzed the experiments. YG provided technical and clinical assistance. JL took part in valuable discussion. CC and SY drafted the manuscript. XH and ZH

revised the manuscript and supervised the research. All authors commented on the manuscript. XH is the guarantor.

Funding This work was supported by grants from the Noncommunicable Chronic Diseases-National Science and Technology Major Project (No. 2024ZD0520404) and the National Natural Science Foundation of China (No.91942313).

Competing interests None declared.

Patient consent for publication Not applicable.

Ethics approval The study conformed to the ethical guidelines and was approved by the Research Ethics Committee of Zhongshan Hospital Fudan University (No. B2021-020R). Participants gave informed consent to participate in the study before taking part.

Provenance and peer review Not commissioned; externally peer reviewed.

Data availability statement Data are available upon reasonable request. The raw bulk RNA-seq data generated in this study have been deposited in the Genome Sequence Archive (GSA) at the National Genomics Data Center (NGDC), China National Center for Bioinformation (CNCB) under accession number HRA011536 (available at: https://ngdc.cncb.ac.cn/gsa-human/). All other original data supporting the conclusions of this article are available from the corresponding author upon reasonable request.

ORCID iD

Changzhou Chen http://orcid.org/0000-0001-5396-3204

REFERENCES

1 Sung H, Ferlay J, Siegel RL, *et al*. Global Cancer Statistics 2020: GLOBOCAN Estimates of Incidence and Mortality Worldwide for 36 Cancers in 185 Countries. *CA Cancer J Clin* 2021;71:209–49.
2 Cucarull B, Tutusaus A, Rider P, *et al*. Hepatocellular Carcinoma: Molecular Pathogenesis and Therapeutic Advances. *Cancers (Basel)* 2022;14:621.
3 Li X, Ramadori P, Pfister D, *et al*. The immunological and metabolic landscape in primary and metastatic liver cancer. *Nat Rev Cancer* 2021;21:541–57.
4 Jain MK, Kashiki S, Hsieh C-M, *et al*. Embryonic Expression Suggests an Important Role for CRP2/SmLIM in the Developing Cardiovascular System. *Circ Res* 1998;83:980–5.
5 Hoffmann C, Mao X, Brown-Clay J, *et al*. Hypoxia promotes breast cancer cell invasion through HIF-1α-mediated up-regulation of the invadopodial actin bundling protein CSRP2. *Sci Rep* 2018;8.
6 Midorikawa Y, Tsutsumi S, Taniguchi H, *et al*. Identification of genes associated with dedifferentiation of hepatocellular carcinoma with expression profiling analysis. *Jpn J Cancer Res* 2002;93:636–43.
7 Wang J, Guan X, Zhang Y, *et al*. Exosomal miR-27a Derived from Gastric Cancer Cells Regulates the Transformation of Fibroblasts into Cancer-Associated Fibroblasts. *Cell Physiol Biochem* 2018;49:869–83.
8 Wang S-J, Wang P-Z, Gale RP, *et al*. Cysteine and glycine-rich protein 2 (CSRP2) transcript levels correlate with leukemia relapse and leukemia-free survival in adults with B-cell acute lymphoblastic leukemia and normal cytogenetics. *Oncotarget* 2017;8:35984–6000.
9 Jerby-Arnon L, Shah P, Cuoco MS, *et al*. A Cancer Cell Program Promotes T Cell Exclusion and Resistance to Checkpoint Blockade. *Cell* 2018;175:984–97.
10 Sammut S-J, Crispin-Ortuzar M, Chin S-F, *et al*. Multi-omic machine learning predictor of breast cancer therapy response. *Nature* 2022;601:623–9.
11 Yang H, Cheng J, Zhuang H, *et al*. Pharmacogenomic profiling of intra-tumor heterogeneity using a large organoid biobank of liver cancer. *Cancer Cell* 2024;42:535–51.
12 Carlson CM, Frandsen JL, Kirchhof N, *et al*. Somatic integration of an oncogene-harboring Sleeping Beauty transposon models liver tumor development in the mouse. *Proc Natl Acad Sci U S A* 2005;102:17059–64.
13 Whittaker S, Marais R, Zhu AX. The role of signaling pathways in the development and treatment of hepatocellular carcinoma. *Oncogene* 2010;29:4989–5005.
14 Yang X, Deng B, Zhao W, *et al*. FABP5^{+} lipid-loaded macrophages process tumour-derived unsaturated fatty acid signal to suppress T-cell antitumour immunity. *J Hepatol* 2025;82:676–89.
15 Ostman A. The tumor microenvironment controls drug sensitivity. *Nat Med* 2012;18:1332–4.
16 Wang S, Su D, Chen H, *et al*. PD-L2 drives resistance to EGFR-TKIs: dynamic changes of the tumor immune environment and targeted therapy. *Cell Death Differ* 2024;31:1140–56.
17 Lopez-Bergami P, Lau E, Ronai Z. Emerging roles of ATF2 and the dynamic AP1 network in cancer. *Nat Rev Cancer* 2010;10:65–76.
18 Gupta S, Campbell D, Dérijard B, *et al*. Transcription factor ATF2 regulation by the JNK signal transduction pathway. *Science* 1995;267:389–93.
19 Castro-Mondragon JA, Riudavets-Puig R, Rauluseviciute I, *et al*. JASPAR 2022: the 9th release of the open-access database of transcription factor binding profiles. *Nucleic Acids Res* 2022;50:D165–73.
20 Siegel RL, Miller KD, Wagle NS, *et al*. Cancer statistics, 2023. *CA Cancer J Clin* 2023;73:17–48.
21 Ohtsuka M, Ling H, Ivan C, *et al*. H19 Noncoding RNA, an Independent Prognostic Factor, Regulates Essential Rb-E2F and CDK8-β-Catenin Signaling in Colorectal Cancer. *EBioMedicine* 2016;13:113–24.
22 Junttila MR, de Sauvage FJ. Influence of tumour micro-environment heterogeneity on therapeutic response. *Nature* 2013;501:346–54.
23 Trédan O, Galmarini CM, Patel K, *et al*. Drug resistance and the solid tumor microenvironment. *J Natl Cancer Inst* 2007;99:1441–54.
24 Tauber AI. Metchnikoff and the phagocytosis theory. *Nat Rev Mol Cell Biol* 2003;4:897–901.
25 DeNardo DG, Ruffell B. Macrophages as regulators of tumour immunity and immunotherapy. *Nat Rev Immunol* 2019;19:369–82.
26 Van Dam H, Wilhelm D, Herr I, *et al*. ATF-2 is preferentially activated by stress-activated protein kinases to mediate c-jun induction in response to genotoxic agents. EMBO J 1955;14:1798–1811.
27 Zhou S-L, Dai Z, Zhou Z-J, *et al*. Overexpression of CXCL5 mediates neutrophil infiltration and indicates poor prognosis for hepatocellular carcinoma. *Hepatology* 2012;56:2242–54.
28 Chen P, Luo X, Dai G, *et al*. Dexmedetomidine promotes the progression of hepatocellular carcinoma through hepatic stellate cell activation. *Exp Mol Med* 2020;52:9.
29 Leung CO, Yang Y, So KK, *et al*. Abstract 1746: Broad-spectrum kinome profiling identifies CDK6 upregulation as a driver of lenvatinib resistance in hepatocellular carcinoma. *Cancer Res* 2023;83:1746.
30 Seehawer M, Heinzmann F, D'Artista L, *et al*. Necroptosis microenvironment directs lineage commitment in liver cancer. *Nature* 2018;562:69–75.